EXP — 164
May 16, 1989

Fermilab

Main Ring Dynamic Aperture Studies

Experimenters: Yu-Chiu Chao, Don Edwards, Helen Edwards, Rod Gerig, Steve Holmes, Gerry Jackson, Sateesh Mane, Mike Syphers, Vladimir Visnjic

Study Periods: Nov. 14-16, Dec. 19-21, 1988

Editor: Rod Gerig

Introduction

The behavior of the Main Ring at the injection energy of 8 GeV has long been a topic of concern. Even before the advent of the Tevatron era at Fermilab it was known that the dynamic aperture was not what had been expected. With the introduction of many new devices into the Main Ring to accommodate the Tevatron and the colliding beam physics program, the performance of Main Ring at 8 GeV deteriorated. Over the past several years simulations of Main Ring have been performed. [1] [2]. Some previous studies have been done to try to reconcile the machine with the model. However it is just in the past year or so that several new tools have become available and reliable enough to use in acquiring dynamic aperture measurements. These are the flying wire system, enabling emittance and momentum spread measurements, and a set of collimators in the injection line into Main Ring which allow the beam to be scraped to a size which can be shown to be smaller than the Main Ring aperture. Furthermore, some of the hardware advances made to the rf system for the colliding beam program have been utilized in these studies. In particular, paraphasing

[1] R. Gerig, S. Pruss, F. Turkot, "Simulations of the Fermilab Main Ring," Proceedings of the 1987 IEEE Particle Accelerator Conference, 1987, pp. 1123

[2] R. Gerig, S. Mane, S. Pruss, M. Syphers, D. Trbojevic, "Improvements to the Fermilab Main Ring," presented at the European Particle Accelerator Conference, Rome, Italy, June 7-11, 1988.

of the rf cavities provides the capability of reducing the rf voltage to very low levels thus limiting the momentum spread of the beam.

The focus of the efforts during the study periods of November and December, 1988 was twofold. First, we attempted to understand and improve the Main Ring aperture. Any improvements that can be made will have immediate benefit to the colliding beam and fixed target programs. Second, we continue the effort of making measurements that will either improve or validate our models of Main Ring performance. A particular motivation at this point is the proposal to replace the Main Ring with a new machine called the Main Injector. It is vital to be able to demonstrate that the Main Injector will perform at its design specification. The modeling done for the Main Injector will certainly evolve from the Main Ring modeling experience due to similarities in beam size, physical aperture size, and injection energies. Therefore this aspect of the studies was referred to as Main Injector studies.

Outline of Report

1. Measurement Techniques
2. Studies Environment
3. Transverse Emittance Growth
   (a) The Diffusion Process
   (b) Beam–Gas Scattering
   (c) RF Noise Measurements
4. Aperture Measurements
   (a) Physical Aperture Measurements
   (b) Dynamic Aperture Measurements
      i. As a function of Tune
      ii. As a function of Resonance Driving Terms
      iii. As a function of $\frac{\Delta p}{p}$
      iv. Evaluation of localized nonlinearities
5. Momentum Aperture Restrictions
   (a) Observation
   (b) Vertical Dispersion Measurement at different tunes
   (c) Operation at tunes of 19.6
6. Operation of Main Ring at 15 GeV/c

(a) Physical Aperture Measurements

(b) Dynamic Aperture Measurements

7. Concluding Remarks

1 Measurement Techniques

Much of the data taken during these study periods involved measuring the acceptance of the machine as various conditions were changed. The technique used in doing so is described here although some of the modeling and background is discussed in a later section dealing with transverse emittance growth.

The traditional method of measuring the acceptance, or dynamic aperture of an accelerator is to inject a small emittance beam and allow it to grow in transverse size. This growth can either be due to natural causes, or can be enhanced through various mechanisms such as noise on beam damper plates. The beam will ultimately reach a final size which will be the largest beam size that the machine can contain. The transverse beam sizes are then measured and the answers are taken to be the machine acceptance. If it is known that the physical aperture is larger than what is measured, then the acceptance is interpreted as the dynamic aperture. In making this measurement one must know when the final, or to use a better term, 'equilibrium' distribution has been reached, and secondly a device to make the measurement must exist and be accurate.

In Main Ring this procedure has been virtually impossible until very recently. As we discovered once we could make the measurements, the dynamic aperture of Main Ring is often smaller than the smallest beam the Fermilab Booster is capable of producing. Even when Main Ring tuning optimizes the dynamic aperture, the relative sizes of incoming beam to Main Ring acceptance are still too similar to allow a clear measurement like the one described above.

Three factors have now made such measurements possible. The first is a set of beam collimators, or scrapers in the 8 GeV transport line between the Booster and Main Ring which allow very small emittance beams to be injected into Main Ring. This of course is done at the expense of intensity. Second, a set of flying wires installed in Main Ring has begun to give believable transverse emittance measurements, even at these low intensities. Flying wires do not measure emittance directly. At best they provide a transverse profile of the beam. From this raw data a Gaussian fit is done which provides a rms (σ) for the distribution. The emittance calculations which assume a knowledge of the lattice of Main Ring are:

$$\frac{\epsilon}{\pi}_{mm-mrad} = \frac{6\sigma^2(\beta\gamma)}{\beta_{lattice}}$$

The emittance is therefore taken to include 95% of the beam by virtue of the factor of six in the numerator. This expression is correct only if there is no dispersion at the location of the measurement. This is true in the vertical plane due to the choice of location of the wire. In the horizontal plane two wires are located at positions of different dispersion, so that the calculation can fit for a momentum spread as well as the transverse distribution.

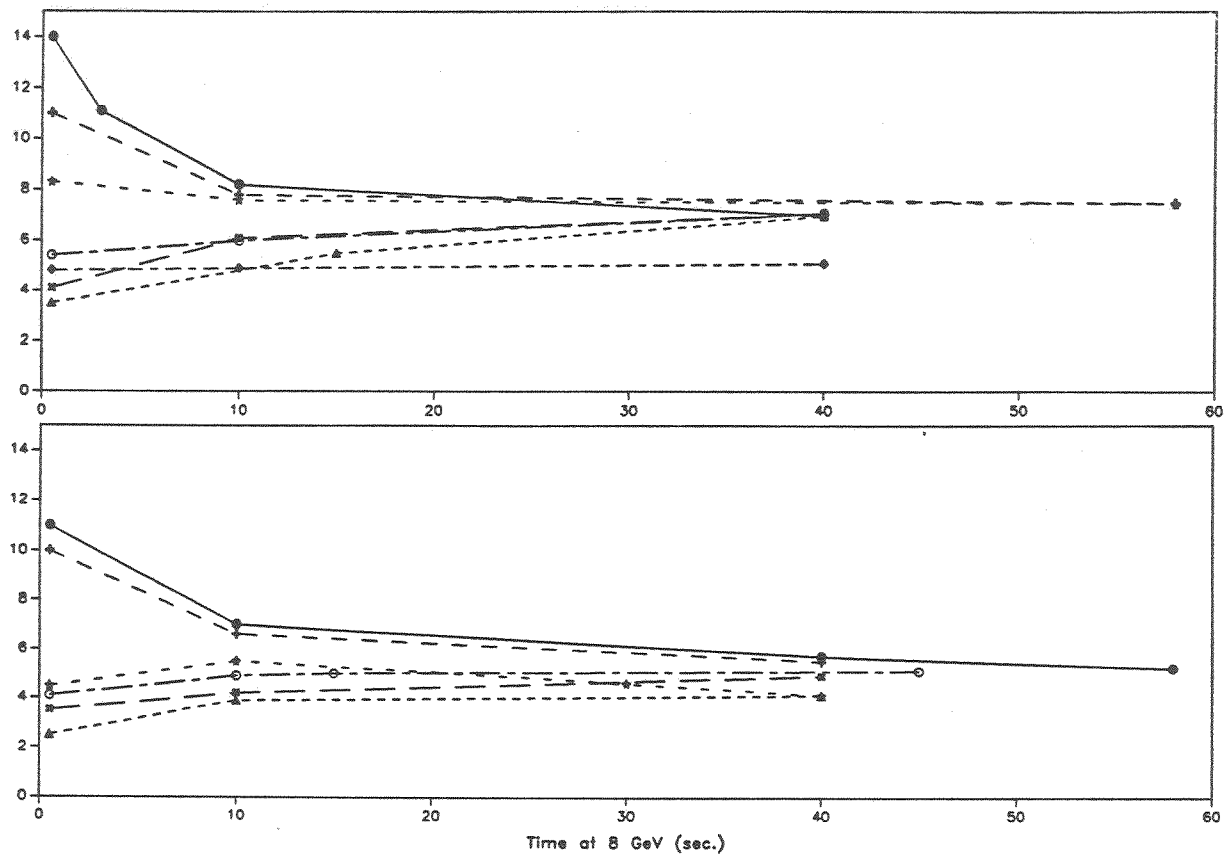

Figure 1: Emittance versus time for beam with different injected emittances.

Finally, we made the somewhat surprising discovery that in order to make these measurements we would need to let the beam coast at 8 GeV for many more seconds than we had previously allowed for. In fact the final equilibrium distribution often is not reached until after 30 to 40 seconds.

Although not used traditionally as a measurement technique, it is known that when a beam larger than the acceptance of the machine is injected it also should achieve the equilibrium distribution after some time (and after some beam loss.) This too was observed in the studies. Figure 1 is a plot of data from wire flies illustrating both the shrinking of the rms for beams with emittances larger than the acceptance of the machine, and the growing of beam the rms in cases when the incoming beam is smaller than the acceptance. Correlated with these observations was an additional quantity, the beam lifetime. Typically the beam intensity signal was plotted on the console using logarithmic scaling. A response in the form of a straight line indicates true exponential decay. We found that when the beam had reached equilibrium size it would exhibit exponential beam loss. Thus a straight line on this plot indicated when it was appropriate to take the flying wire emittance data. Figure 2 illustrates this. The beams injected with sizes larger than the acceptance initially show beam loss faster than exponential. Beams injected with smaller emittances lose beam more slowly while growing to the size of the machine acceptance. It also turns out that the final lifetime is proportional to the machine acceptance as will be discussed in the section

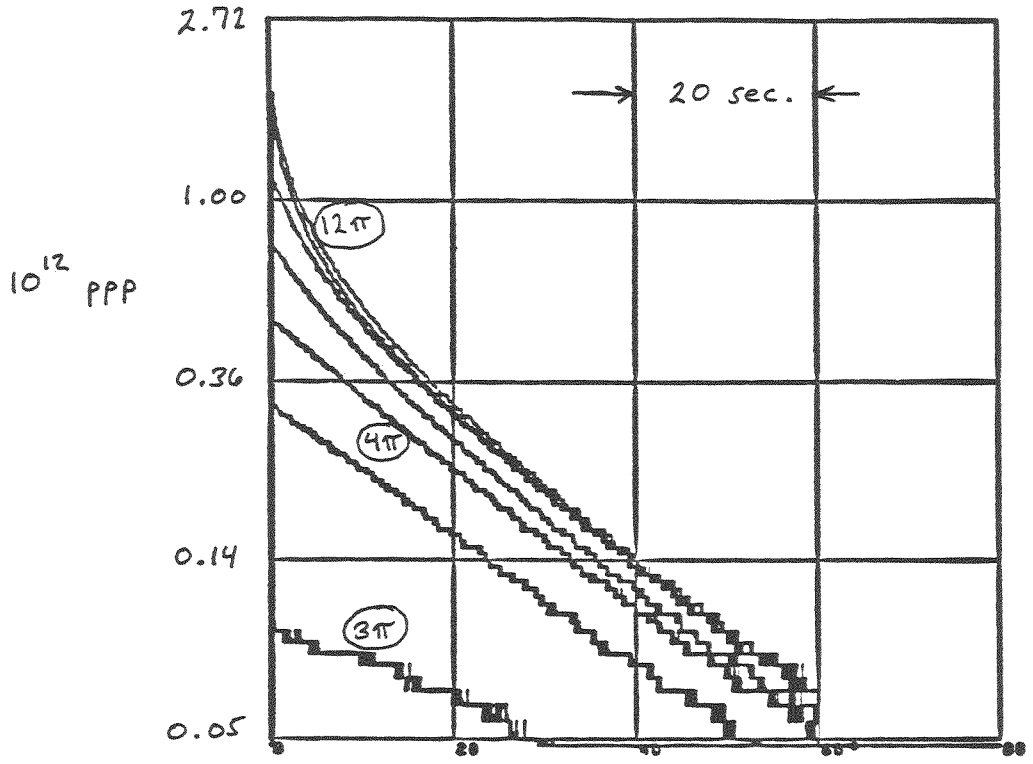

Figure 2: Beam intensity versus time for beam with different injected emittances.

on emittance growth.

Once a number of these measurements had been done, it was no longer necessary for the beam scrapers to be moved into the beam; accurate measurements of equilibrium parameters could be taken with the larger incoming beam.

2 Studies Environment

The Main Ring studies were done parallel to studies in the Tevatron, and at times it was necessary to deliver beam to the Tevatron upon demand. We found it desirable to use a time-line which had a 2B Main Ring cycle at the beginning, the kind of Main Ring cycle used for Tevatron injection. This was followed by a 29 cycle in that it is the kind of Main Ring cycle which normally precedes any beam injection into the Main Ring, and therefore leaves the remanent fields in their most familiar state. This was followed by the 60 second, 8 GeV cycle used for our studies. A 2D reset was chosen due to the fact that a 2D cycle is defined as an 8 GeV DC ramp, and therefore requires fewer changes to be put into a studies mode. Several 29 ramps completed the 120 second supercycle. In order for measurements to be made we found it necessary to turn off the low and high frequency transverse beam dampers, and the rf feedback loops (radial position control). If any of these were left on, sharp beam loss occurred during the 60 second cycle, usually after 10 seconds into the cycle. We did not explore the reason for the beam loss because it seems to impact neither operation nor the measurements we were intent on taking. Beam was injected using a range of intensities from the booster.

The studies done at 15 GeV/c were performed utilizing a special ramp which was assigned for the course of these studies to a 21 reset type. Main Ring power supply limitations allow no ramp specification longer than 16 seconds, thus a ramp was defined with a 15 GeV/c front porch lasting a few seconds which then went on to 120 GeV. A new console applications program was written which waited for the 15 GeV/c front porch, and then put the power supply system into a storage mode. After 60 seconds the storage mode was released allowing the ramp to continue. This ramp occupied the same slot in the time-line that the 8 GeV DC ramp had occupied. Other conditions for the 15 GeV/c measurements were similar to those at 8 GeV with the exception of the rf feedback loops. At the time of the studies it was not possible to turn them off after having used them to accelerate to 15 GeV/c. Because of this, beam loss was again observed associated with the functioning of the loops. This will be rectified if future 15 GeV/c studies are to be done.

3 Transverse Emittance Growth

As illustrated in Figure 1, the emittance of the 8 GeV coasting beam tends to vary as a function of time until an equilibrium value is reached. The mechanism causing the emittance variation and the cause of the limiting emittance are the two fundamental aspects of this process that must be investigated. In this section we attempt to interpret the emmitance

behavior in terms of a diffusion process. [3] Diffusion rates for two important processes, beam-gas scattering and RF noise, are predicted. Measurements indicate that the beam-gas scattering plays a major role in the emittance behavior while growth due to RF noise is negligible.

3.1 The Diffusion Model

We wish to discuss the general behavior of particle distributions in the presence of mechanisms which continuously stimulate emittance growth. To begin with, we write the beam phase space distribution function, $f(x, x', t)$, in terms of the Courant-Snyder invariant $W = (x^2 + (\alpha x + \beta x')^2)/\beta \equiv r^2/\beta$ so that $f = f(W, t)$. The diffusion equation is thus of the form

$$\frac{\partial f}{\partial t} = D \frac{\partial}{\partial W} \left(W \frac{\partial f}{\partial W} \right)$$

where D, the diffusion constant, is the average rate of change of W with respect to time. If the emittance growth is caused by the changing of a particle's direction due to fluctuations in magnetic fields, elastic scattering off of residual gas particles, etc., then the diffusion constant is identified as

$$D = \langle \frac{d}{dt} (\beta dx'^2) \rangle = \bar{\beta} \dot{\theta}^2_{rms},$$

where $\dot{\theta}^2_{rms}$ is the time average rate of change of the variance of the change in transverse slope inflicted by the particular mechanism.

To proceed, we define two quantities:

$$\begin{aligned} Z &= \frac{W}{W_a} \\ \tau &= \left(\frac{D}{W_a} \right) t \end{aligned}$$

where W_a is the Courant-Snyder invariant corresponding to the aperture of the machine (i.e., the admittance). If a is the half-aperture at a particular location where the amplitude function has the value β, then $W_a = a^2/\beta$. Notice that Z and τ are both dimensionless quantities.

In terms of Z and τ, the problem reduces to

$$\frac{\partial f}{\partial \tau} = \frac{\partial}{\partial Z} \left(Z \frac{\partial f}{\partial Z} \right)$$

subject to the boundary conditions

$$f(Z, 0) = f_o(Z)$$

$$f(1, \tau) = 0.$$

[3] Teng, L. C., "Pressure Dependence of the decay of the Main Ring Coasting Beam," EXP-1, Fermilab Internal Report, 1972.

The solution of the above differential equation is

$$f(Z,\tau) = \sum_n c_n J_o(\lambda_n \sqrt{Z}) e^{-\lambda_n^2 \tau/4}$$

with

$$c_n = \frac{1}{J_1(\lambda_n)^2} \int_0^1 f_o(Z) J_o(\lambda_n \sqrt{Z}) dZ$$

where λ_n is the nth zero of the Bessel function $J_o(z)$.

We now consider a particular form of the initial distribution, namely a bi-gaussian in $x - x'$ phase space. For this situation, the function f_o will be

$$\begin{aligned} f_o(x,x')dxdx' &= \frac{1}{2\pi\sigma^2} e^{-(x^2+(\alpha x+\beta x')^2)/2\sigma^2} \beta dx dx' \\ &= \frac{1}{2\pi\sigma^2} e^{-r^2/2\sigma^2} r dr d\theta \\ &= \frac{1}{2} e^{-r^2/2\sigma^2} d(r^2/\sigma^2) \end{aligned}$$

or,

$$f_o(Z)dZ = \frac{a^2}{2\sigma^2} e^{-(a^2/2\sigma^2)Z} dZ.$$

So, the coefficients c_n become

$$c_n = \frac{\alpha}{J_1(\lambda_n)^2} \int_0^1 e^{-\alpha Z} J_o(\lambda_n \sqrt{Z}) dZ,$$

where $\alpha = a^2/2\sigma^2$.

Figure 3 shows how $f(Z,\tau)$ varies with time for the case $\sigma/a = 0.20$. The particle distribution grows in transverse size until it reaches the aperture (Z=1) at which time the area under the curve quickly begins to decrease. The intensity $N(\tau)$ for this same case is displayed in the second part of Figure 3. From $\tau = 0$ to $\tau \approx 0.1$ the intensity is relatively constant. Upon reaching the aperture limit, the intensity rapidly falls off until $\tau \approx 0.5$, where the final lifetime $4/\lambda_1^2$ is reached.

When a substantial fraction of the initial Gaussian distribution lies outside the aperture limit (all particles with $Z > 1$ being lost immediately) the rather flat region of $N(Z)$ for small Z disappears. Figure 4 shows the intensity vs. time for the case $\sigma/a = 0.4$. The lifetime, determined by

$$\tau_L(\tau) = -\frac{N(\tau)}{dN/d\tau}$$

is shown in the adjacent figure for the two cases $\sigma/a = 0.2, 0.4$. The one case begins with a very long lifetime which then decreases to the value $4/\lambda_1^2$, while the other case begins with a very short lifetime and rapidly approaches its asymptotic value.

The dimensionless quantity τ is related to time t by

$$\tau = \left(\frac{D}{W_a}\right) t$$

and hence the asymptotic lifetime in real time units is given by

$$t_L = \frac{4}{\lambda_1^2} \frac{W_a}{D}.$$

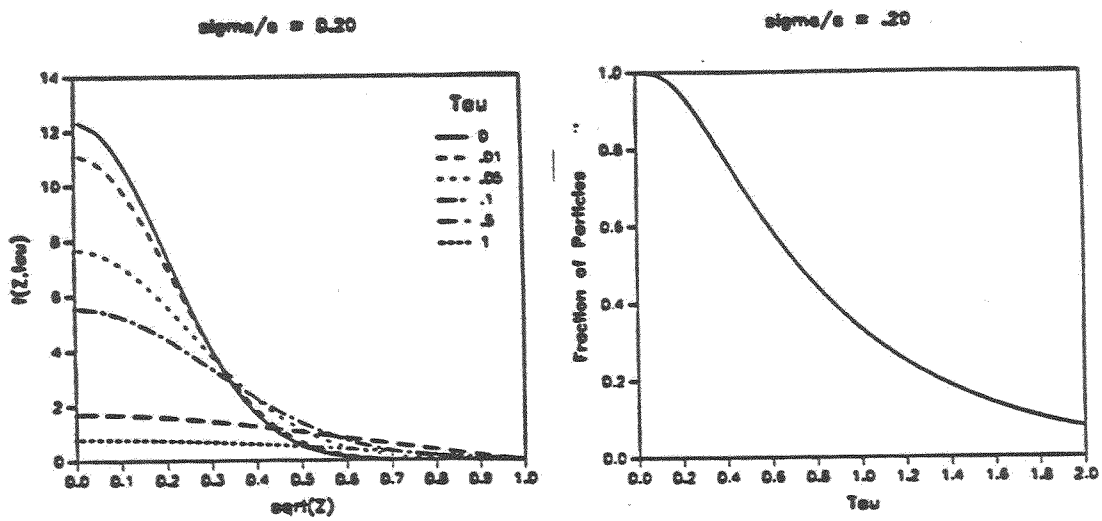

Figure 3: Particle distribution and beam intensity as functions of time.

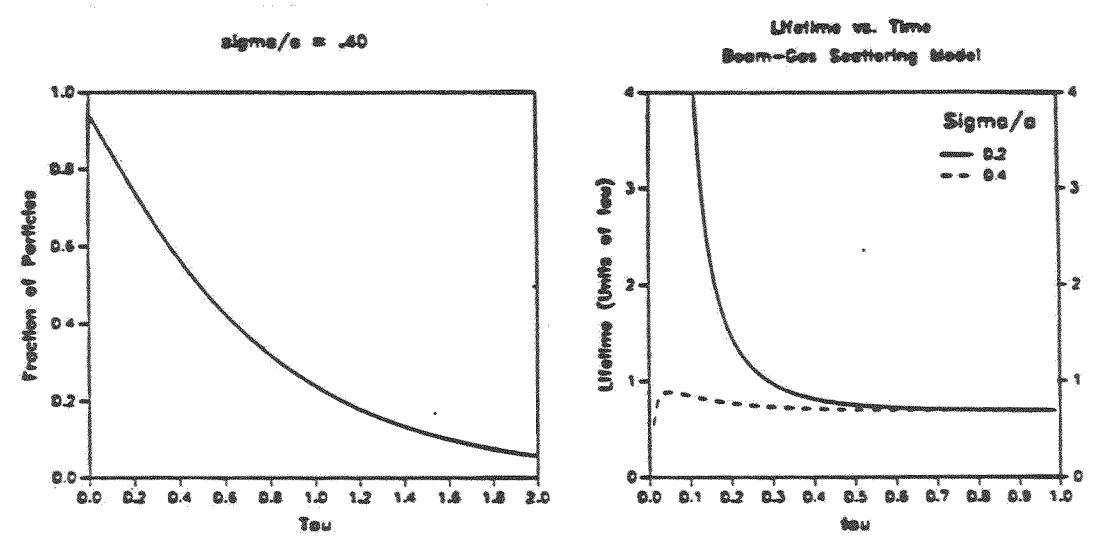

Figure 4: a) Beam intensity vs. time for large incoming beam emittance. b) Lifetime vs. time for large and small beams.

3.2 Beam-Gas Scattering

For particles scattering off of the residual gas in the vacuum chamber, the average rate of change of the transverse scattering angle in one degree of freedom, $\dot{\theta}^2_{rms}$, is given by

$$\dot{\theta}^2_{rms} = \left(\frac{15MeV}{pv}\right)^2 \frac{c}{L_{rad}}$$

where L_{rad} is the radiation length of the residual gas constituent. The rate of emittance growth may thus be written as

$$\langle\frac{d\epsilon}{dt}\rangle = \bar{\beta}\left(\frac{15MeV}{E_o}\right)^2 \frac{c}{\gamma^2}\frac{1}{L_{rad}}$$

For the Main Ring, the average value of the amplitude function is $\bar{\beta} \approx 50$ m.

Recent measurements of the Main Ring vacuum [4] show that the primary constituents of the residual gas are hydrogen (41.0%), water (37.7%), and nitrogen/carbon-monoxide (13.5%). The radiation lengths of these substances at STP are: [5]

H_2:	$L_o =$	6800 m
H_2O:		360 m
N_2:		300 m

Thus, in terms of the average vacuum pressure around the ring, $p[\mu torr]$,

$$\frac{1}{L_{rad}} = (2.0 \times 10^{-12}/m) \cdot p[\mu torr].$$

With an average ring pressure of $0.14\mu torr$ as deduced from the ion pump readings, the expected emittance growth rate due to beam-gas scattering is

$$\begin{aligned}\langle\frac{d\epsilon}{dt}\rangle &= (50m)(15/938)^2\frac{3\times10^8 m/sec}{(9.47)^2}(0.14)(2.0\times10^{-12}/m)\\ &= 12\times10^{-9}m/sec.\end{aligned}$$

During the studies of 10/4/88, emittance and lifetime measurements were performed for the 8 GeV beam at equilibrium, thus giving a direct measure of the diffusion constant:

$$\begin{aligned}\langle\frac{d\epsilon}{dt}\rangle &= \frac{4}{(2.405)^2}\frac{\hat{\epsilon}/\pi}{t_L} = \frac{4}{(2.405)^2}\frac{4.8\times10^{-6}m}{(9.47)(27sec)}\\ &= 13\times10^{-9}m/sec\end{aligned}$$

in very good agreement with the beam-gas prediction.

In order to verify that the emittance growth was indeed due to beam-gas scattering, an experiment was performed on 11/14/88 in which the vacuum pressure in the Main Ring was

[4] D. Trbojevic, technical memo, FNAL, 14 February 1989.

[5] from "Review of Particle Properties," Phys. Letters 170B, April, 1986.

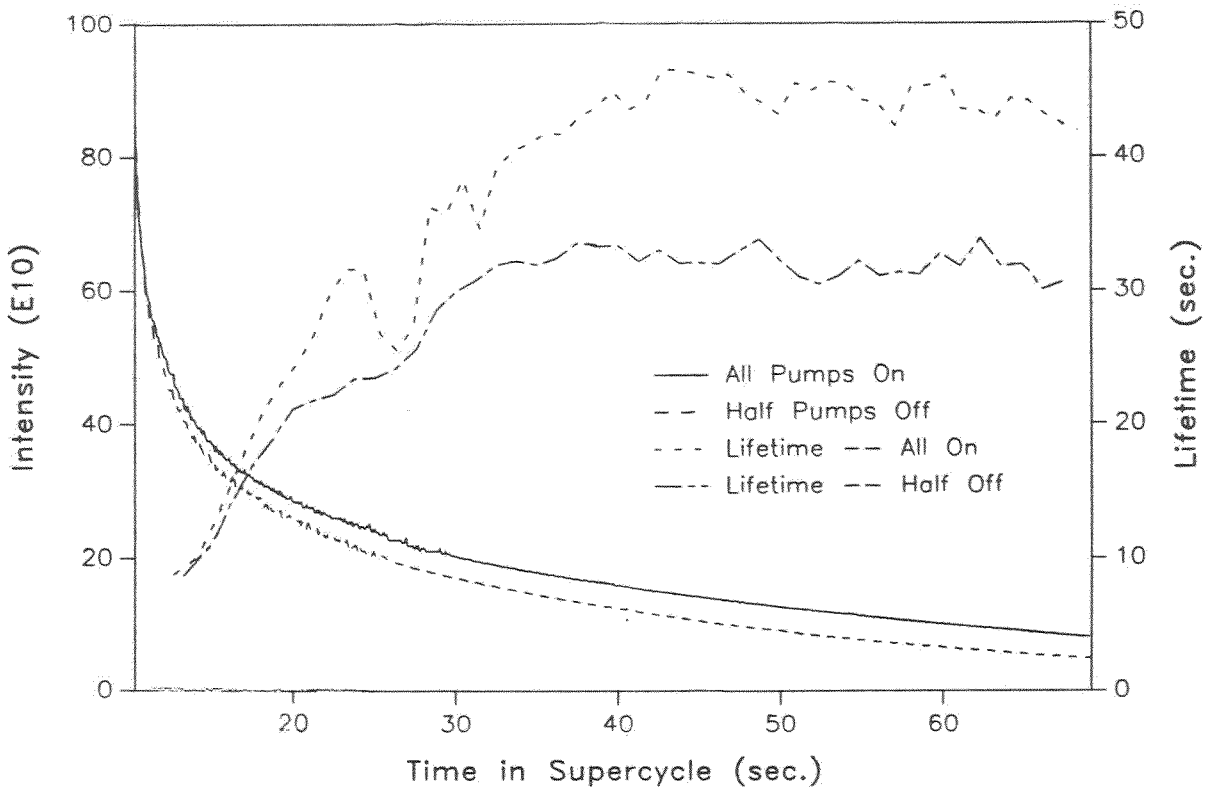

Figure 5: Beam-gas lifetime experiment.

altered and the change in beam intensity lifetime noted. The average pressure that the beam sees, $\langle p \rangle$, is related to the average of the pressures at the pump locations, $\bar{p}_p$, by

$$\langle p \rangle / \bar{p}_p \approx 1 + 0.06L = 1.4$$

for the standard 6 m pump spacing. At the beginning of this experiment, $\bar{p}_p = .10\mu torr$ and so $\langle p \rangle_1 = .14\mu torr$. Under this condition, the equilibrium lifetime and emittance were measured to be $\tau_1 = 43sec$, and $\hat{\epsilon}\gamma = 9.5\pi$ mm-mr.

Next, every other Main Ring ion pump was turned off and about one hour was spent waiting for equilibrium to return. After this time, the average pump pressure was measured to be $\bar{p}_p = .12\mu torr$ giving $\langle p \rangle_{1/2} = (1 + .06 \cdot 12)(.12) = .21\mu torr$. Therefore, we expected to see a new equilibrium lifetime $(.14/.21) = .67$ times smaller than the original lifetime. Indeed, the measured lifetime was 31 sec. (.72 times smaller) and the equilibrium emittance remained at 9.5π. The raw intensity data as well as the computed lifetimes are shown in Figure 5.

3.3 RF Noise

Though the arguments of the previous subsection suggest that the observed emittance growth in the Main Ring at injection is caused by beam-gas scattering, it has been observed

in the past (as well as during these studies) that turning off the RF system affects the beam lifetime. We would like to see if this effect is due to the dynamic aperture changing when the RF is turned off, or whether it is due to the removal of a source of RF noise which has been affecting the emittance growth.

The emittance growth rate due to random noise in the RF system may be written as[6]

$$\langle \frac{d\epsilon}{dt} \rangle = \pi f_o \mathcal{H} \frac{e^2 \langle v^2 \rangle}{E^2}$$

where $\sqrt{\langle v^2 \rangle}$ is the rms voltage due to noise in the accelerating system and f_o is the revolution frequency. The quantity $\mathcal{H}$ is given by [7]

$$\mathcal{H} = \gamma D^2 + 2\alpha D D' + \beta D'^2$$

where D and D' are the dispersion function and its slope and α, β, γ are the Courant-Snyder [8] parameters at the location of the RF cavities.

In the case of RF voltage noise, the differential equation describing the response of a single small amplitude particle is given by

$$\ddot{x} + \omega^2(1 + \alpha cos(2\omega_\alpha t))x = 0$$

where α is the amplitude of the frequency (tune) modulation component at the angular frequency $2\omega_\alpha$. The solutions to this equation are called Mathieu functions[9], and have very strong nonlinear responses when $\omega = 2\omega_\alpha, 3\omega_\alpha, \ldots$. In the case of weak modulation at $2\omega_\alpha$ we find that[10]

$$\dot{\epsilon} = \frac{\pi}{4} f_o \left(\frac{\eta \omega_{rf}}{E\Omega} \right)^2 cos^2\phi_s \, (eV_{rms})^2 \, \epsilon$$

where ϕ_s is the synchrotron phase, ω_{rf} is the angular RF frequency, Ω is the angular synchrotron frequency, η is the momentum compaction, and V_{rms} is the rms RF voltage fluctuation.

Figure 6 shows the power spectrum of the RF voltage near the RF frequency. The top photograph is over a range of 10 kHz per division. Assuming a dominant phase noise contribution, at the betatron frequency (19 kHz) the rms phase amplitude is approximately 5x10-5 radians. This translates into an invariant 95% emittance growth rate of approximately $4 \times 10^{-5} \pi mm - mrad/sec$, far too slow to be of any significance. The voltage noise induced emittance growth rate is similarly negligible. On the other hand, the power near the synchrotron frequency (bottom photograph) is much greater, and may cause measurable longitudinal emittance growth. [11]

---

[6] S. Mane and G. Jackson, Nucl. Instr. and Meth. In Phys. Research A276, 8 (1989)

[7] M. Sands, SLAC-121, 131 (1970)

[8] E. D. Courant and H. S. Snyder, Ann. Phys. 3, 1 (1958)

[9] M. Abromowitz and I. Stegun, Handbook of Mathematical Functions, Dover Publications, New York (1972).

[10] S. Mane, private communication

[11] G. Dome, CERN 84-15, 215 (1984)

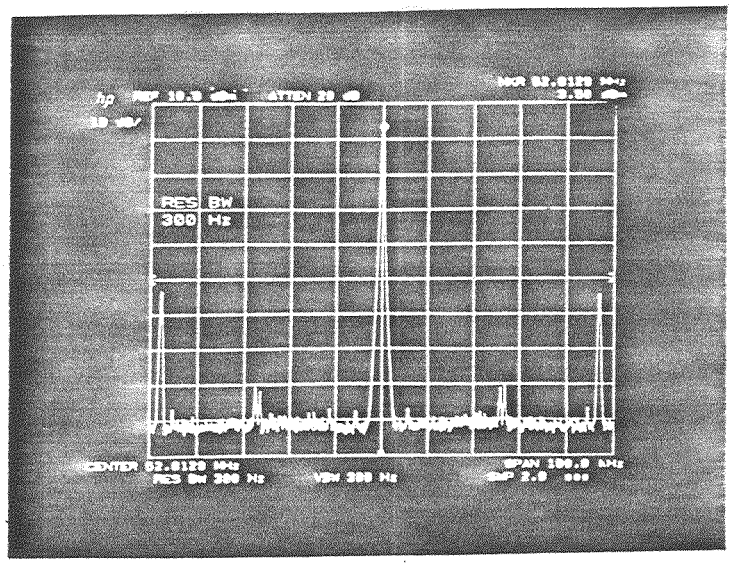

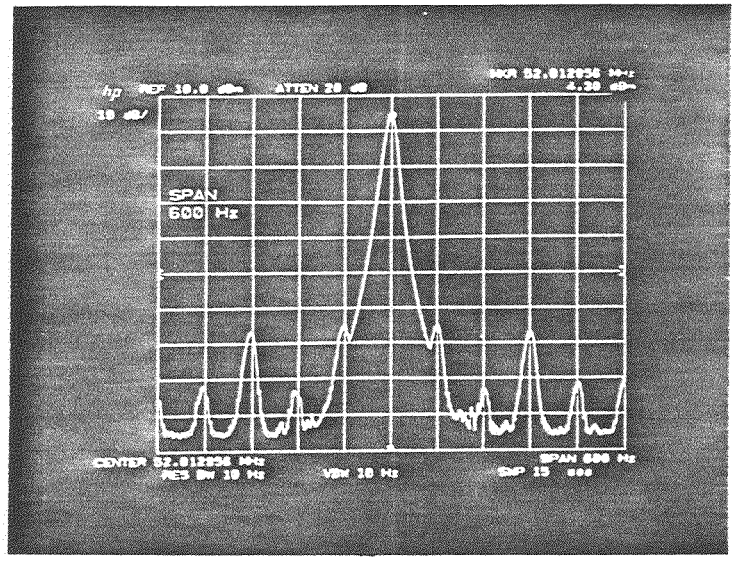

Figure 6: Power spectra of Main Ring RF Voltage. The vertical scale is 10 db/div, the horizontal scale are 10 kHz (top) and 60 Hz (bottom) per division

In addition to observing the noise power in the RF voltage directly, beam admittance and lifetime measurements were made under a variety of RF conditions. Of relevance here are measurements where the RF was either on or off, where either a collimator or the normal Main Ring admittance limited emittance growth, and where the chromaticity was either low or high.

Figure 7 contains the data. High chromaticity is actually -15 units, and low chromaticity is -3 units. Since the relationship between equilibrium diffusion rate, admittance, and lifetime is roughly $D = \frac{A}{\tau}$, concentrate on the data with the scrapers in. In this case A is constant, and the beam loss rate is proportional to the diffusion rate. In figure 7, for both chromaticities, we see that τ is independent of the existence of RF. Therefore, RF noise plays no role in the observed Main Ring diffusion rate. On the other hand, looking at the data where the normal Main Ring aperture is accessible, note that the RF-off data shows consistently better beam lifetimes than the RF-on data. Comparing the slopes of the lines in the plots, which are proportional to the diffusion rate, there does seem to be a correlation between larger chromaticities and smaller diffusion rates.

3.4 Quadrupole Modulation

The synchrotron oscillations particles execute produce two distinct effects in the betatron planes. The first is a modulation of the closed orbit via the dispersion function around the ring, the second is tune modulation due to chromaticity. In order to distinguish between the two effects, a sine wave generator was connected to a quadrupole, and the frequency was set to near the synchrotron frequency. The result appears in figure 8, in the same fashion as the RF noise data in figure 7. The chromaticity was set to -3 units during all of the measurements. As was the case in figure 7, in the absence of Main Ring collimators the modulation-off and -on data exhibited identical lifetimes. The amplitude of the quadrupole modulation was chosen such that it equalled the tune variation a $\sigma p/p$ particle makes in a lattice with a chromaticity of 10 units. By comparing figures 7 and 8, note that the diffusion rate for this quadrupole modulation falls between the observed low and high chromaticity rates. The conclusion based on this data is that tune modulation is not a dominant dynamic aperture effect, though it may have and effect on the diffusion rate. Other sections deal with the effects of closed orbit dependences.

4 Aperture Measurements

4.1 Physical Aperture Measurements

To determine the physical aperture of the Main Ring, the beam was kicked using the pulsed kicker magnet normally used for the tune measurement process. The BPM turn-by-turn system was used to record beam centroid position and beam intensity over the first thousand turns after the kick. An example of such a measurement is shown in Figure 9.

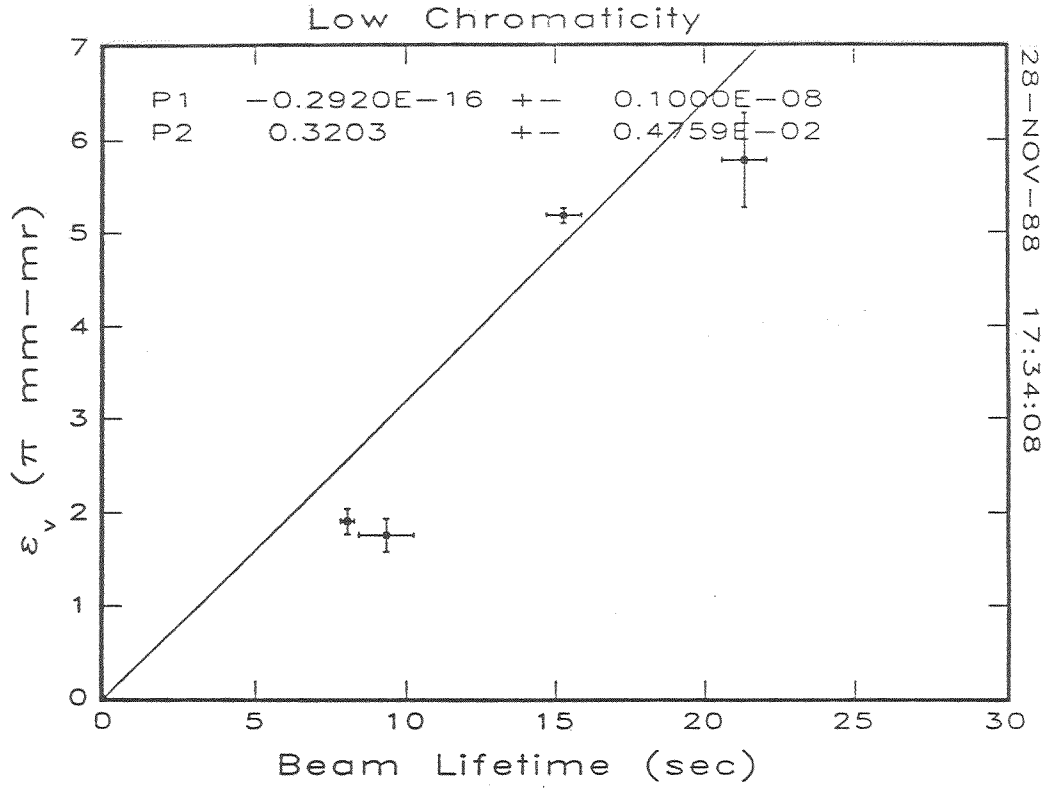

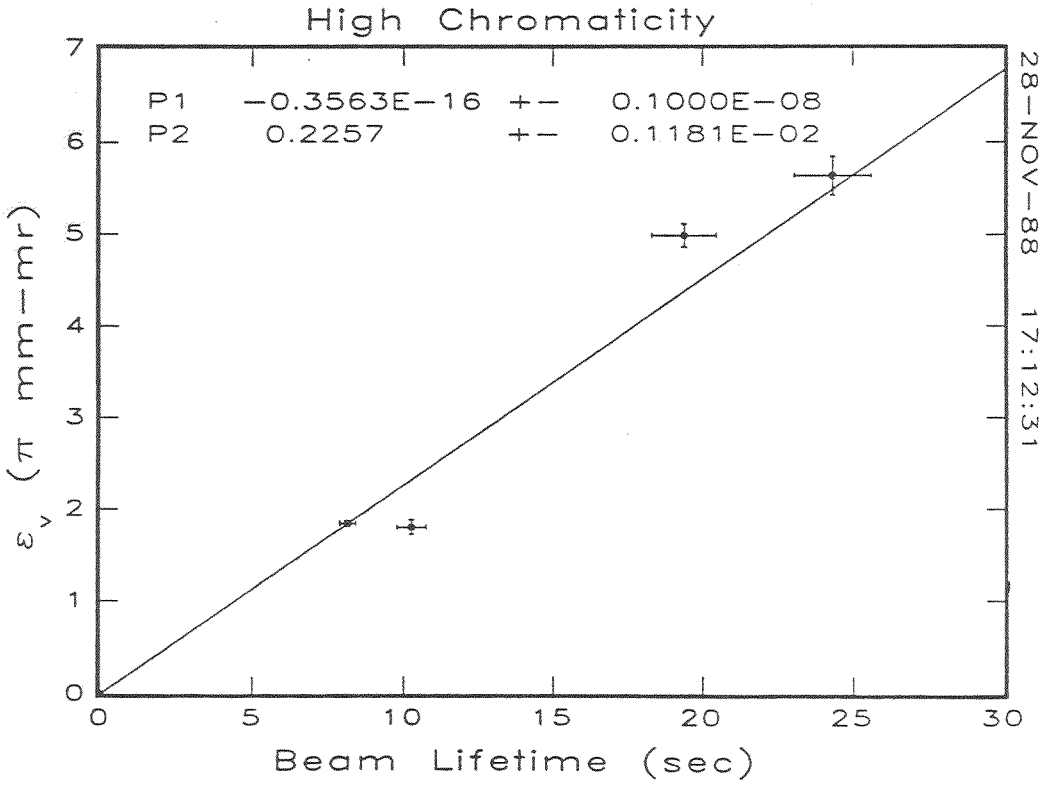

Figure 7: Main Ring admittance vs. beam lifetime for low (top) and high (bottom) chromaticity with scrapers in (left set of points) and out (right set of points). The dark points are RF-on data, the open points RF-off.

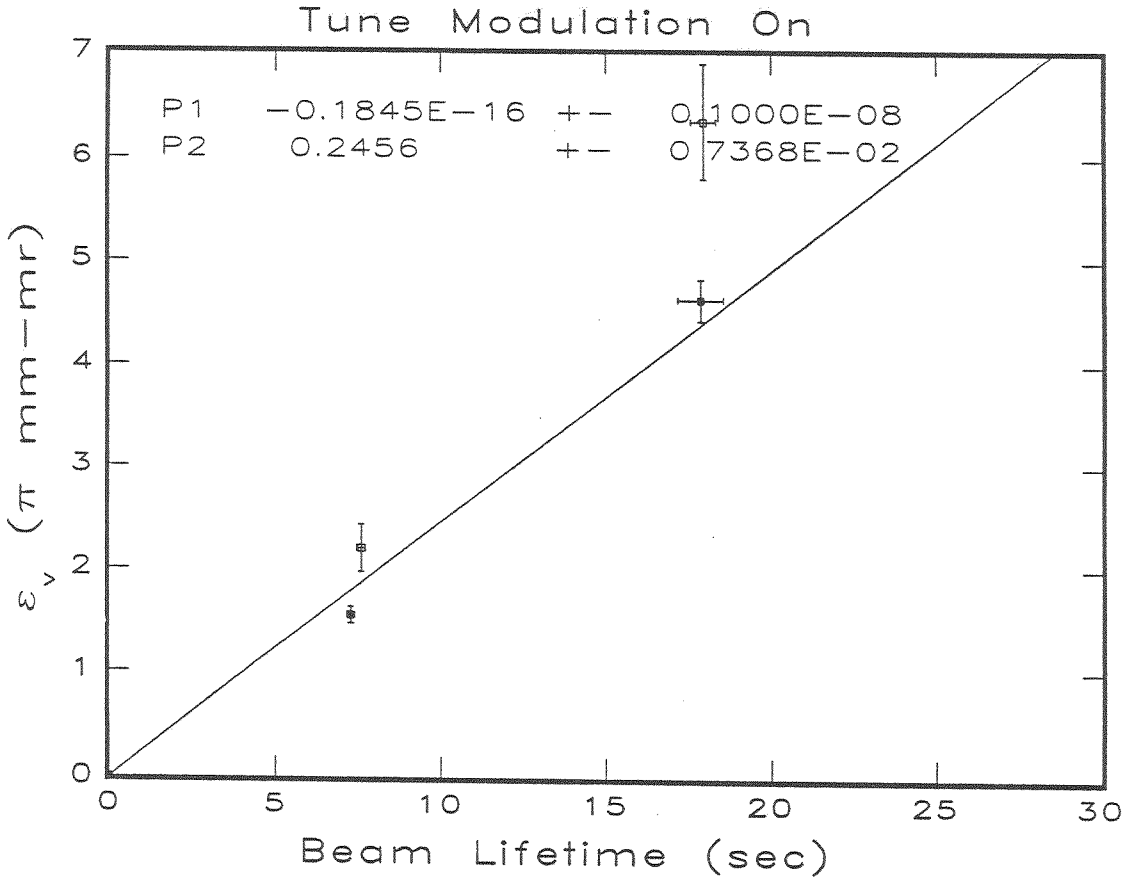

Figure 8: Effect of tune modulation introduced via an oscillating quadrupole. Dark points represent modulation-on data, open points modulation-off.

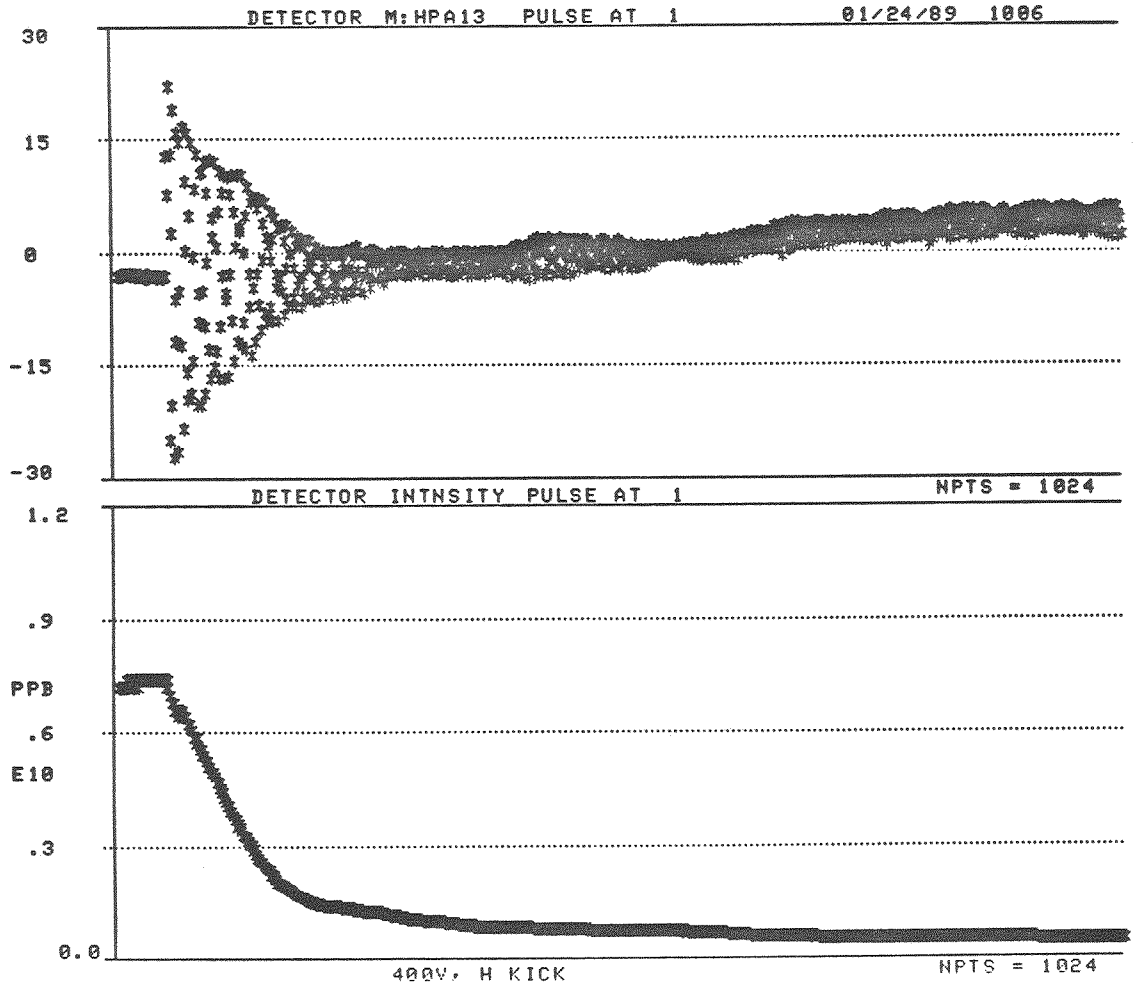

Figure 9: Typical BPM turn-by-turn data. The top plot shows the beam centroid position as a function of turn number. The bottom plot shows the beam intensity.

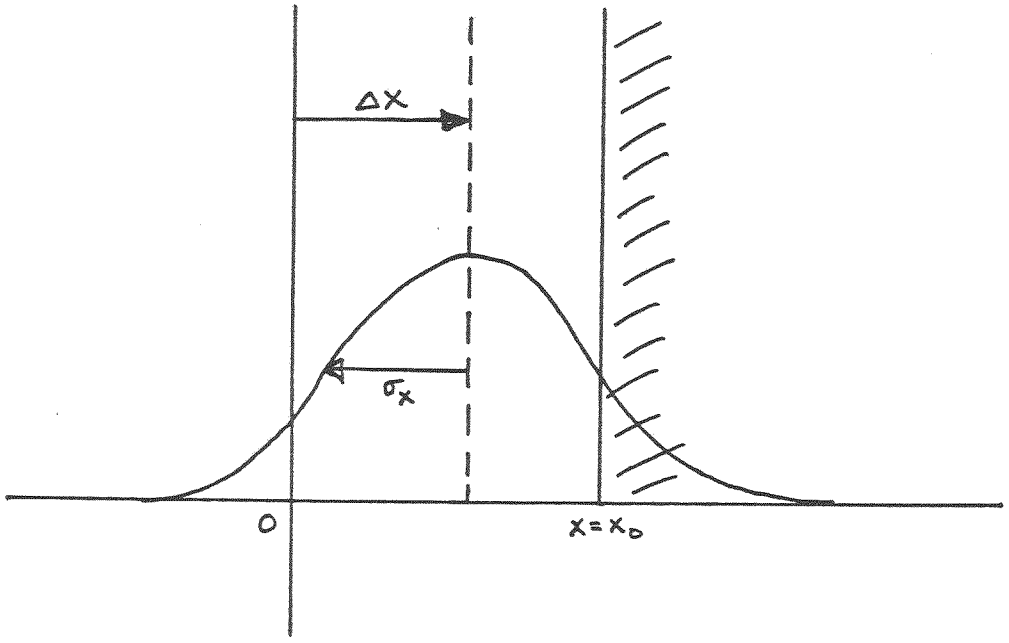

Figure 10: Physical aperture experiment definitions.

From the position data, a kick amplitude can be obtained. From the intensity data, the fraction of the beam lost due to the kick is measured. We denote the kick amplitude by Δx and the fraction of particles that survive the kick after one thousand turns by $I_{1000}/I_0 \equiv P(\tilde{x})$. From Figure 10, we see that if the beam distribution is assumed to be Gaussian, the fraction of surviving particles is given by

$$P(\tilde{x}) = \int_{-\infty}^{\tilde{x}} \frac{1}{\sqrt{2\pi}} e^{-u^2/2} du$$

where

$$\tilde{x} = \frac{x_o - \Delta x}{\sigma_x}.$$

By measuring Δx and $P(\tilde{x})$ (and hence $\tilde{x}$) one may then deduce the beam size σ_x at the location of the physical aperture x_o.

The above experimental technique was applied during the studies shift of 24 January 1989. The data are shown in Table 1 and Table 2. In the tables, Δn is the number of turns it took for the intensity to drop from its initial value I_0 to the value $(I_0 + I_{1000})/2$. The horizontal and vertical kicks are given at the same location in the lattice, where $\beta_x/\beta_y \approx 3$, and so the vertical deflections are not as large as those in the horizontal plane. A problem with the vertical kicker power supply prevented vertical amplitudes greater than 10 mm from being reached.

Fitting the above measured values of Δx,$\tilde{x}$ and Δy,$\tilde{y}$ yield

$$\sigma_x = 6.5mm, \qquad x_o = 16.4mm$$

Table 1: Horizontal Physical Aperture Measurements

$\Delta x(mm)$	$P(\tilde{x})$	$\tilde{x}$	Δn
0	1	—	—
6.6	.94	1.56	500
10.3	.81	0.88	110
13.3	.66	0.42	70
16.9	.48	0.06	70
19.3	.31	-0.50	70
21.0	.14	-1.09	60
24.9	.06	-1.56	60
27.4	.07	-1.47	50
29.1	$< .02$	-2.05	1
29.3	.05	-1.64	2

Table 2: Vertical Physical Aperture Measurements

$\Delta y(mm)$	$P(\tilde{y})$	$\tilde{y}$	Δn
0	1	—	—
1.7	1	—	—
2.3	1	—	—
3.4	.98	2.05	500
4.4	.96	1.76	500
5.1	.94	1.56	500
6.3	.90	1.28	500
6.8	.92	1.40	500
7.6	.86	1.08	230
8.9	.84	0.99	150
9.1	.81	0.87	130

$$\sigma_y = 5.0mm, \quad y_o = 13.3mm$$

for beam sizes and apertures. The vertical beam size is in agreement with flying wire measurements made during these studies, whereas the horizontal beam size is somewhat larger than that measured by the flying wires (which say that $\sigma_x \approx 5.5mm$ at a typical high dispersion location). It should be noted that if only the horizontal data for which $-1 < \tilde{x} < 1$ are used, then the results are $\sigma_x = 5.5mm$, $x_o = 15.9mm$, though the fit is not quite as good.

We thus conclude that the horizontal physical aperture under the present machine conditions is about 16 mm, while the vertical physical aperture is about 13 mm. These results are in agreement with a somewhat similar experiment that was performed in March of 1987. At that time the apertures were found to be $x_o = 16mm$, $y_o = 12mm$. If we express these apertures in terms of a normalized beam emittance then the corresponding admittances are

$$admittance_x = \pi \frac{x_o^2}{\beta_o} \gamma = 24\pi mm - mr$$

$$admittance_y = \pi \frac{y_o^2}{\beta_o} \gamma = 16\pi mm - mr.$$

4.2 Dynamic Aperture Measurements

Many dynamic aperture measurements were made over the course of the studies periods. The data was compiled and will be presented in four categories representing four of the questions we hoped to explore.

4.2.1 Dynamic Aperture as a function of Tune

Some of the data presented in this section were taken while intentionally doing a scan of tunes. Other data are added from measurements taken throughout the studies periods. The locations in the tune diagram at which data were taken are shown in Figure 11. The lifetimes and acceptances are shown in Figure 12 where the data is plotted versus the location in the tune diagram. The fifth integer resonance lines are clearly shown to be sources of a reduction in the dynamic aperture. This is the clearest measurement to date of the effect of the fifth integer resonance lines. For reasons explained later we choose to run above these lines. Indeed, the point to which the operators regularly tune the machine is point H.

4.2.2 Dynamic Aperture as a function of Driving Term Compensation

The Main Ring is equipped with correction sextupoles and quadrupoles which can be powered to correct for certain third integer and half integer driving terms. It has been customary to use machine study time to retune these elements to improve the 8 GeV efficiency with the machine set to the tunes the elements are compensating for. Typically this study is done first by varying the tunes along a line parallel to but removed from the diagonal (Figure 13). As the tunes are varied, the machine efficiency is measured. In this case the machine efficiency is the amount of the beam that survives about one second at 8 GeV. This initial scan, shown in Figure 14 is taken so that the effectiveness of the tuning can

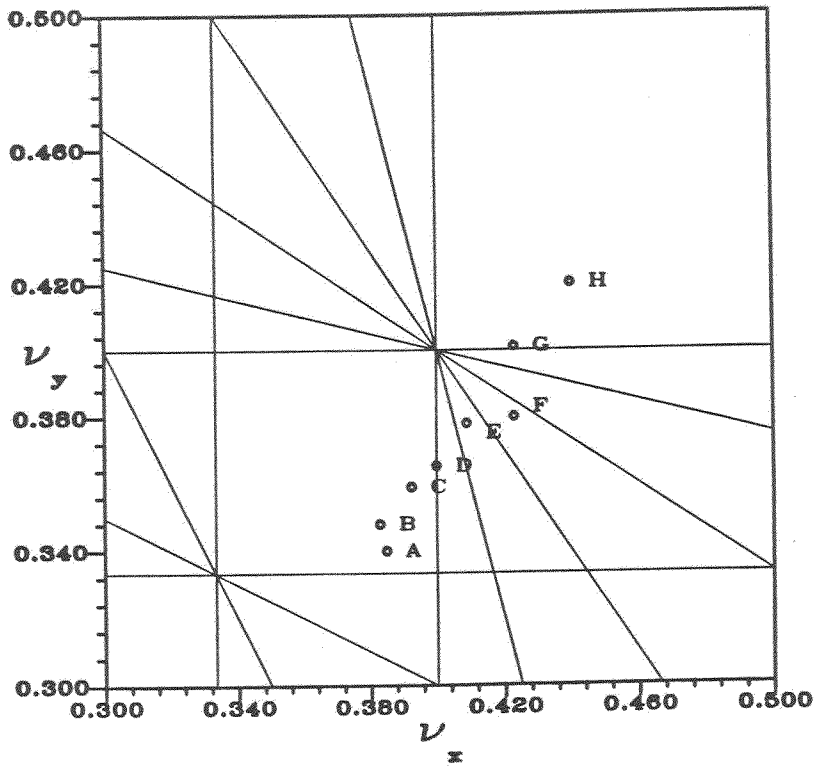

Figure 11: The locations in the tune plane where dynamic aperture measurements were taken

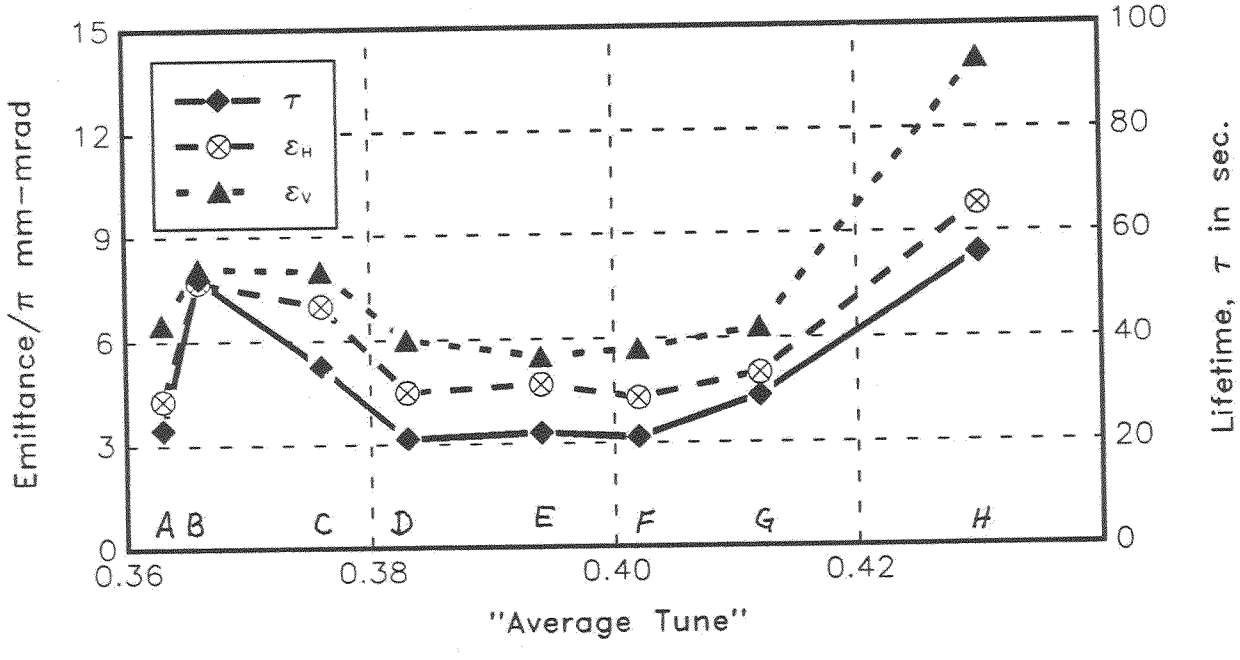

Figure 12: Dynamic aperture measurements as a function of location in the tune plane

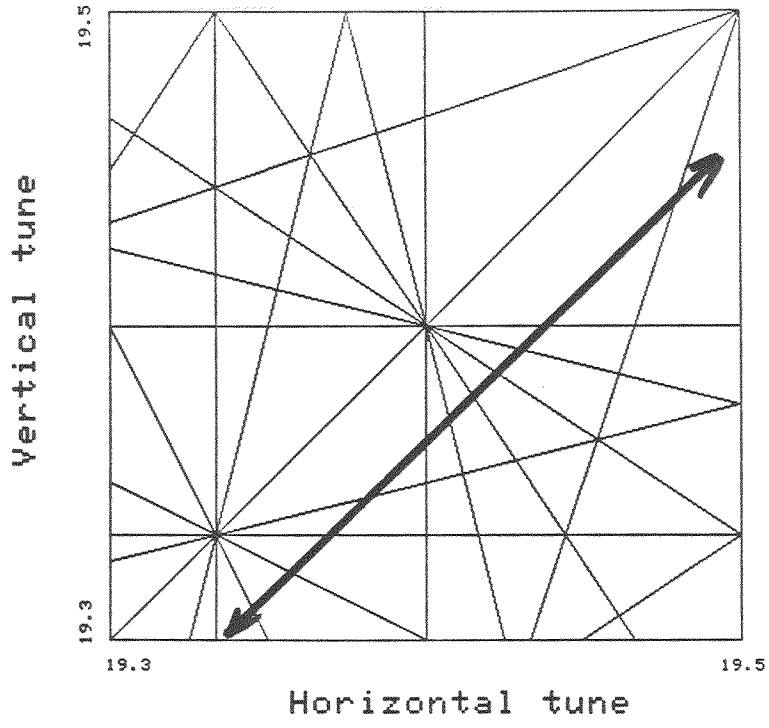

Figure 13: Tune plane showing the scan line used in study

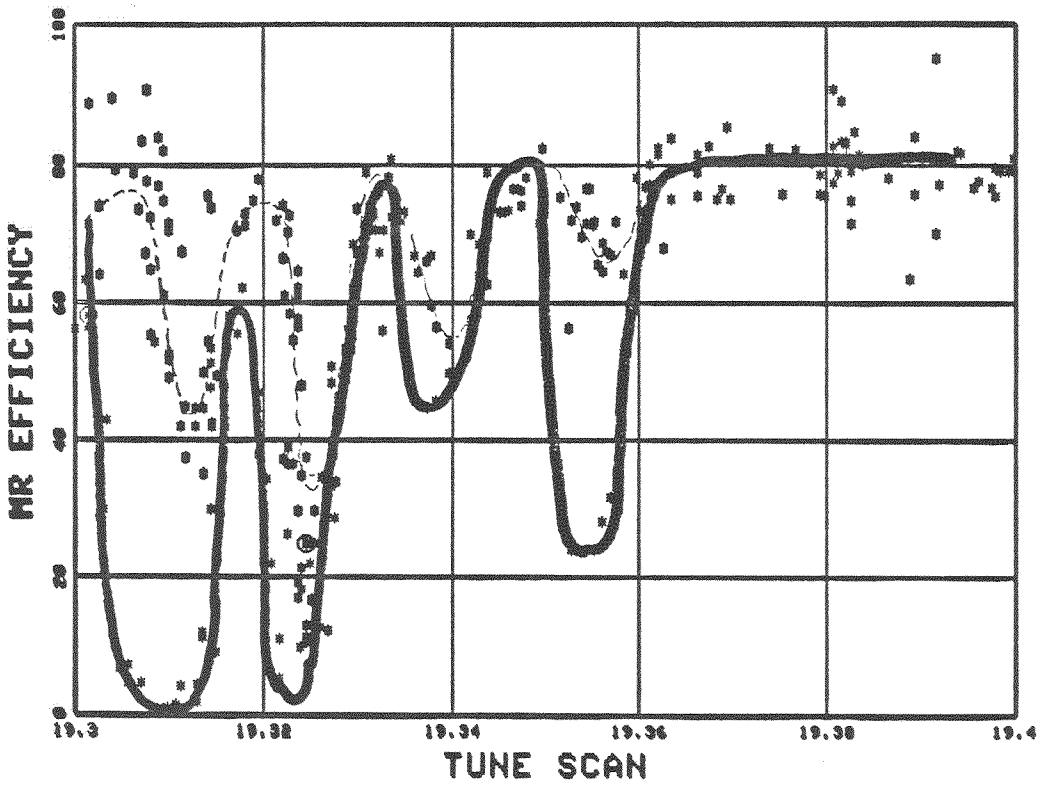

Figure 14: Resonance scan before (solid line) and after (dotted line) compensation. The abscissa is averaged tunes.

be evaluated by comparison with a scan done after the compensations. Following this, the machine tune is set to each of the resonances, and the correctors are tuned for maximum efficiency.

This study was done in the context of the dynamic aperture measurements for several reasons: this was the first opportunity to use the collimators in this study. We hoped the smaller beam would be a more precise probe allowing better resolution of individual resonance lines (previously, and during this study period the compensations and scans were done with the rf off to reduce momentum effects). Secondly, we wanted to see if we could see measurable differences in the dynamic aperture as a result of the compensations. When viewed in the traditional way, the compensations were very successful. Figure 14 shows the scan after the compensations and as can be seen, each of the four third integer resonance lines is less evident. However, dynamic aperture measurements done at tunes away from the resonance lines indicated that the dynamic aperture was unchanged by these compensations.

4.2.3 Dynamic Aperture as a function of $\frac{\Delta p}{p}$

The chromaticity measurements study the machine as a function of $\frac{\Delta p}{p}$. As the momentum is varied the tune changes as a result of the momentum dependent strength of the quadrupoles and as a function of the nonlinear components of the magnetic field experienced by the beam. In Main Ring the relationship between tune and momentum is neither flat nor linear. Thus, to obtain the data in Figure 15, the momentum was varied and the main quadrupoles were readjusted at each step to reset the tunes to $\nu_H = .432$, and $\nu_V = .445$. The shape of the lifetime curve is not surprising, but the large difference seen between the horizontal and vertical equilibrium emittances on the outside of the machine is not understood. However it should be noted that these measurements were taken without allowing time for the establishment of the equilibrium distributions.

4.2.4 Evaluation of Localized Nonlinearities

Among the many modifications made to Main Ring during the past eight years has been the installation of Lambertsons to facilitate injection into and extraction from the Main Ring. These can introduce localized nonlinearities in two ways. First, they can be sources of nonlinearities themselves. The Lambertsons at the abort and at F17 both have current in them when beam is injected at 8 GeV. Secondly, all of the Lambertsons necessitate large (20 mm) displacements at 8 GeV. The resulting closed orbit passes through nearby dipoles in regions where the field is known to be quite nonlinear, and certainly different than what particles on the closed orbit experience elsewhere. Several different studies were devised to examine these effects.

During the November study period special ramps were generated for the F17 and D49 Lambertsons. These ramps provided current in the Lambertsons for the duration of the time that beam was at 8 GeV. The current was chosen to be five times greater than what is normally in the F17 Lambertson at injection. Dynamic aperture and lifetime measurements were made in each case. In the case of the F17 Lambertson no difference between the reference machine data, and the machine with the Lambertson on could be detected in either lifetime of

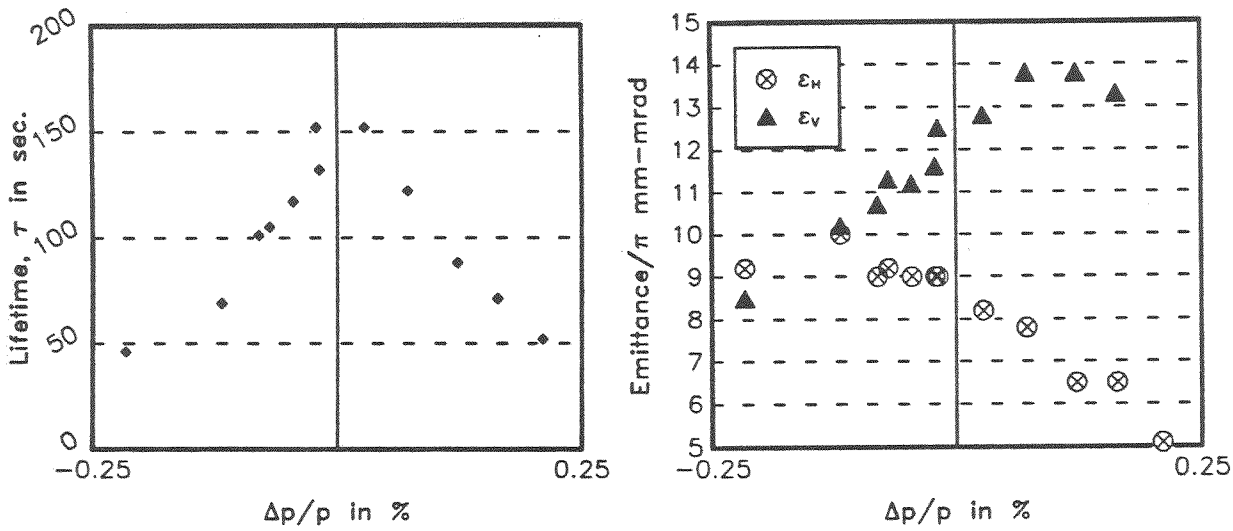

Figure 15: Lifetimes and Emittances as a function of momentum at constant tunes

equilibrium emittances. With current in the D49 Lambertson, a large global orbit distortion was created. To determine if the loss in aperture was due to the orbit distortion, or to the nonlinearity in the Lambertson field, a similar orbit distortion was produced using a nearby correction dipole. The results are presented below.

Measurement	Lifetime	ϵ_H/π	ϵ_V/π
Reference Machine	22 sec.	4.7 mm-mrad	5.5 mm-mrad
D49 Lambertson on	16 sec.	3.3 mm-mrad	4.9 mm-mrad
dipole orbit distortion	21 sec.	4.2 mm-mrad	5.2 mm-mrad

From the D49 data above one might conclude that the nonlinear fields in the Lambertson are effecting the beam. However it is noted that this Lambertson is not powered when the beam is at 8 GeV during normal operation. The conclusion was that the magnetic field nonlinearities in the Lambertsons themselves are not sufficient to cause a reduction in the dynamic aperture. Later in the studies sessions we realized more fully that the position in the tune diagram that this data was taken at, namely $\nu_H = .409$, and $\nu_V = .378$ is a very poor operating point. It might be that if a better point had been used, one associated with a larger dynamic aperture we would have observed a larger effect. It is felt however that the conclusions would not be different.

Several experiments were done to test the second part of the Lambertson question of whether the local bumps move the beam into bad field regions of nearby dipoles. Attempts to remove the bumps so that the closed orbit was centered through all dipoles were unsuccessful. This was in spite of the precautions taken to make sure that there was no current in the Lambertsons, and the use of the collimators to produce small emittance beams that according to calculations should fit through the Lambertsons with the beam centered. By unsuccessful we mean that any attempt to remove these bumps resulted in beam loss that were not attributable to dynamic aperture effects. A second approach was attempted by introducing yet another orbit distortion into the ring at a point similar (in the lattice) to the distortion at F17. A distortion was introduced at C17 of comparable magnitudes. At the time of this study we had learned more about the good operating points and were doing our measurements at one. Therefore the reference machine is much different than in the earlier table, and the measurement is more sensitive.

Measurement	Lifetime	ϵ_H/π	ϵ_V/π
Reference Machine	38 sec.	9.0 mm-mrad	12.5 mm-mrad
C17 at +22.5 mm	35 sec.	9.7 mm-mrad	13.3 mm-mrad
C17 at -36 mm	31 sec.	9.6 mm-mrad	12.0 mm-mrad

Based on these measurements the distortion would not appear to be a problem. Two comments should be made; a three bump was used in this measurement rather than a four bump which is the case at F17-F19; a four bump displaces the orbit in more of the main dipoles. Also there remains the possibility that there is a particularly bad magnet in the F17 region which might make the circumstances different. The study which involves removing (or at least centering) the F17 Lambertsons has been contemplated but not yet done. For the moment we are looking at the question of single orbit distortions in the simulations before pursuing this rather disruptive study.

5 Momentum Aperture Restrictions

Main Ring is unique in accelerators because of the overpasses. As a result there is a non-zero vertical dispersion function which is very localized. In particular there are three locations in the vicinity of the B0 overpass where the vertical dispersion function is greater than 2.0 meters. The nature of the vertical dispersion is different from what one is accustomed to experiencing with horizontal dispersion. This is manifested in two ways. First, the vertical dispersion is a stronger function of tune than is the horizontal. This is because there are only two sources of vertical dispersion separated by many degrees of phase advance. As the vertical tune is changed form 19.35 to 19.65 as it was during the studies, the phase advance between the two sources changes by 36°. Thus the peak values are influenced by the tune change. Second, in the case of localized dispersion peaks it may be many thousands of

revolutions before the betatron phase and synchrotron phase conspire to send a particle into the physical aperture at this point. Simulations have shown that a particle will suddenly be lost at this location of large vertical dispersion after surviving for long periods of time without emittance growth.

In the recent modification of the D0 overpass which reduced the vertical dispersion function it was planned that the Main Ring would eventually operate at higher tunes of 19.6. This would further reduce the vertical dispersion in the B0 region. As of yet this has not been used operationally. Although we had not planned on looking at the vertical dispersion during these studies, it appears that some of the observed effects may be explained by its tune sensitivity. In the next few sections we discuss the initial observations in this series of studies which pointed in this direction, a measurement of vertical dispersion and some results of attempting to run at tunes of 19.6.

5.1 Observation of Problem

In the course of measuring the dynamic aperture as a function of tune during the November studies sessions we encountered a phenomenon which initially went unexplained. With Main Ring adjusted to tunes of $\nu_H = .38$, and $\nu_V = .35$ we measured a dynamic aperture on the order of 8π mm-mrad and a lifetime of 56 seconds. With tunes of $\nu_H = .409$, and $\nu_V = .378$ the dynamic aperture was around 5π mm-mrad and the lifetime was 21 seconds. The anomaly was that with the lower tune values the beam exhibited a sharp loss during the first four seconds of the cycle. Figure 16 shows both traces. Although four seconds is short compared to the 60 second cycle used for these studies it is much longer than the beam spends at 8 GeV during operation, and it is also longer than beam sits at 8 GeV during the resonance scan studies. Evidently this effect is more important than dynamic aperture (as defined earlier) to normal operation, and it will mask attempts to measure dynamic aperture when the measurement is done as described in the section on resonance scans.

In the period of time between the November studies and the December studies we tried to understand this effect based on the data in hand. Going on the assumption that it was related to the vertical dispersion we used the momentum spread numbers produced by the flying wire fits. Although there was considerable variation in the momentum spread numbers from the flying wires, there was a clear pattern. At the lower tune values the momentum spread was smaller and decreased with time. At the higher tune values the momentum spread was larger and increased with time. This was consistent with the assumption that the large beam loss observed in the first four seconds at the lower tune values was due to the particles with larger momentum errors being scraped off at the locations of large dispersion.

In order to explore this question in more detail we arranged, during the December studies, to reduce the rf voltage adiabatically after beam was injected and in so doing reduce the momentum spread of the beam. The longitudinal emittance corresponding to two booster turns is .08 eV-sec. In the Main Ring a rf bucket of the same magnitude occurs with a voltage of 20 kv and produces a *peak* momentum spread of under $.4 \times 10^{-3}$ which is to be compared with an *rms* momentum spread of $.6 \times 10^{-3}$ which is normally observed in Main Ring with two booster turns. During the December studies the Main Ring was set to the

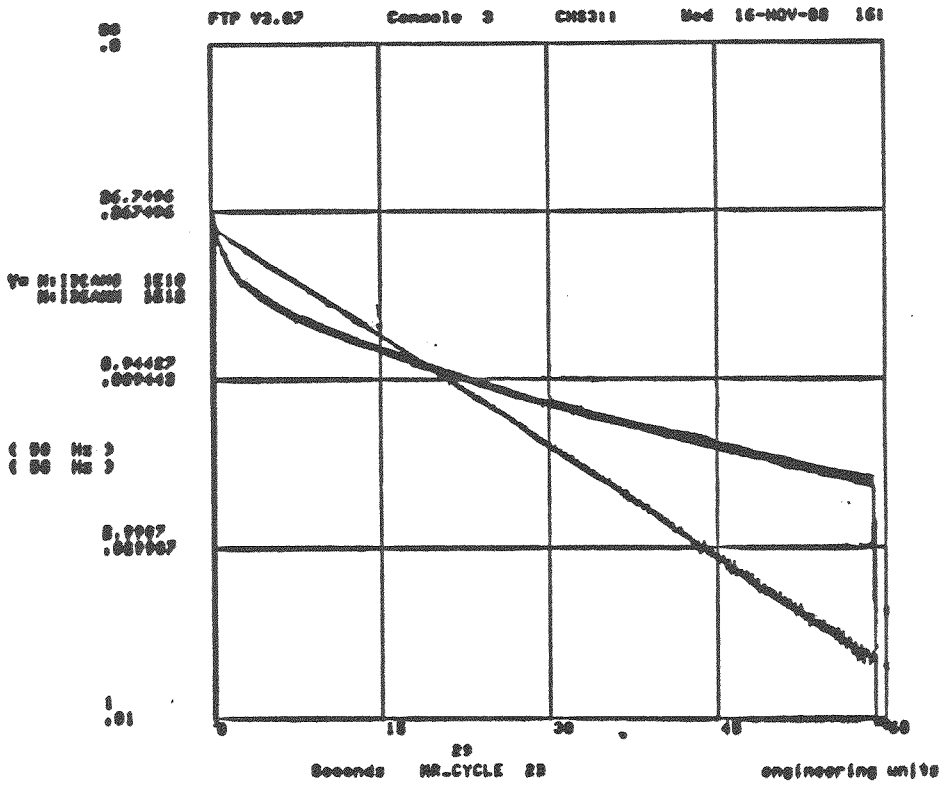

Figure 16:
Beam intensity traces at two different tune values. The trace that is more linear following injection is at tunes of $\nu_H = .409$, and $\nu_V = .378$ and is associated with a smaller dynamic aperture than the second trace which is at tunes of $\nu_H = .38$, and $\nu_V = .35$. The immediate fast loss indicated by this second trace is not explained by dynamic aperture considerations.

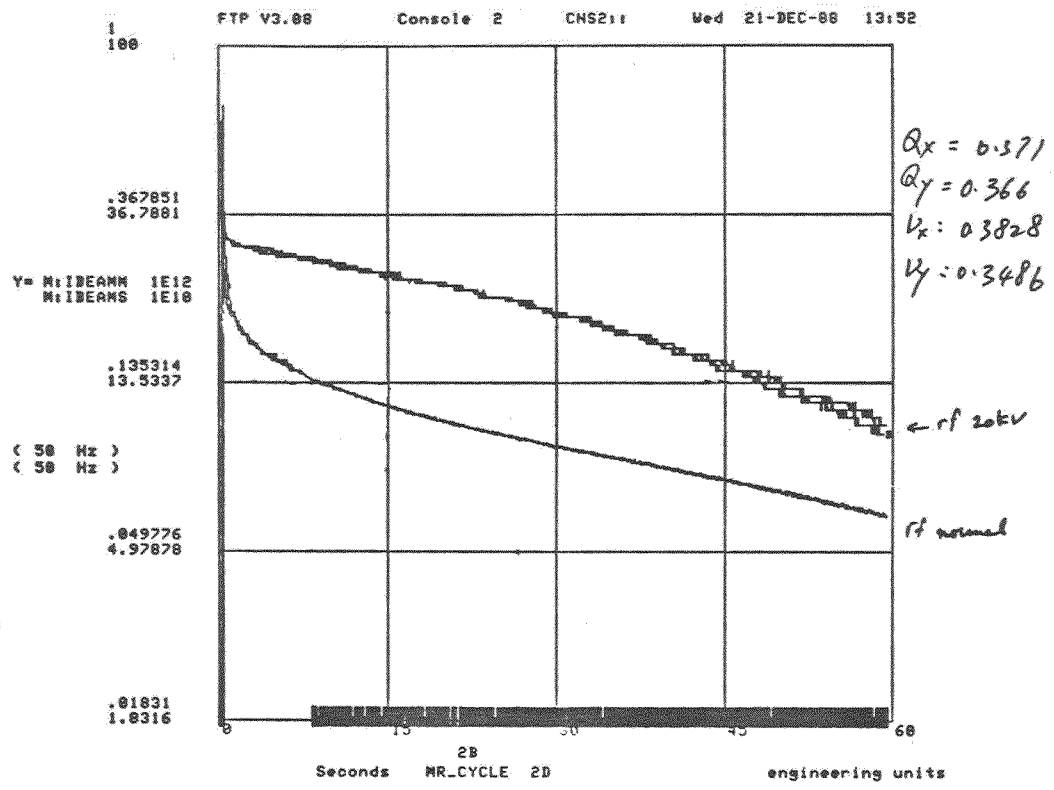

Figure 17: Beam intensities at tunes of $\nu_H = .38$, and $\nu_V = .35$. The rf is at the normal voltage of 500 kv for the lower trace, and 20 kv for the upper trace

lower tune values of $\nu_H = .38$, and $\nu_V = .35$ and with the rf at normal voltage the lifetime and equilibrium emittances were found to be similar to those measured in November. Then the rf was turned down as explained, and the early loss disappeared as shown in Figure 17. If the same experiment is done at higher values of vertical tune the final lifetime and equilibrium emittances are more strongly affected than the early loss.

5.2 Vertical Dispersion Measurement at Different Tunes

A measurement was made to test the prediction that the peak vertical dispersion in Main Ring is a function of vertical tune. At each of the two tune values the rf was programmed to accelerate the beam to the inside, and decelerate it to the outside. At each of these momenta several closed orbits were taken. The horizontal difference orbits were used to calculate the momentum offset. The corresponding vertical displacement at the position i was then used to calculate the vertical dispersion, Y_p, at that location by

$$Y_{p_i} = \frac{y_i}{\frac{\Delta p}{p}}$$

Figure 18 shows the calculated vertical dispersion function for Main Ring. The three peaks in the function occur at locations denoted as A43, A49 and B16. Figure 19 shows the calculated values of the dispersion function at these locations as a function of vertical tune. Measurements of the vertical dispersion were taken at four different values of ν_V. The

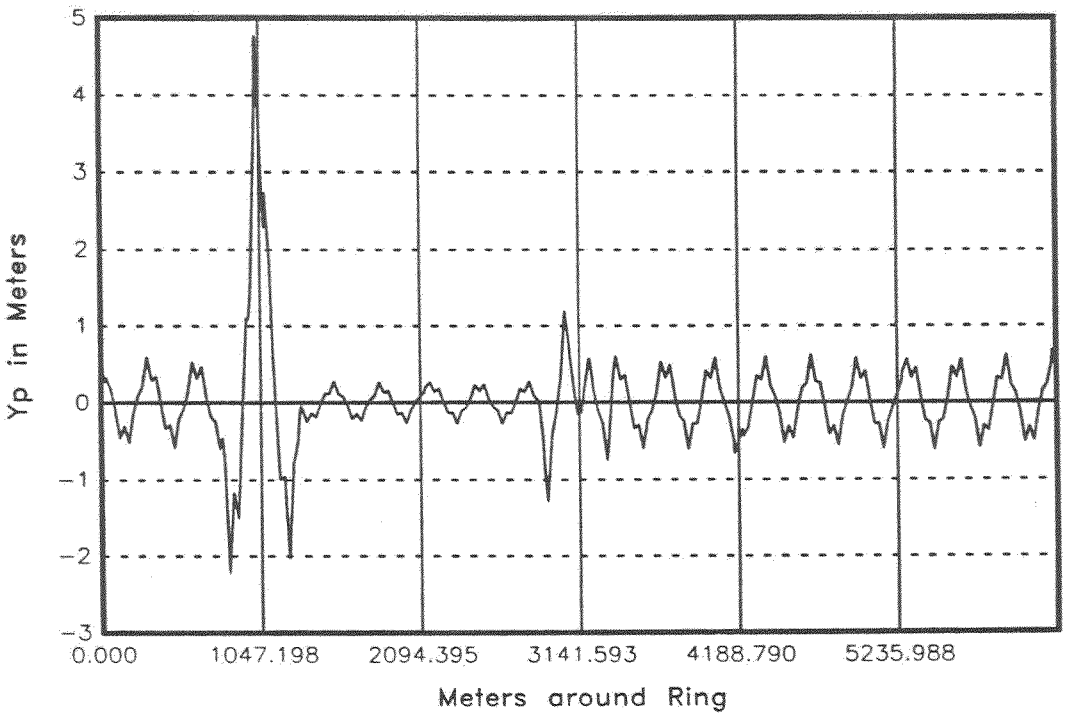

Figure 18: Main Ring Vertical Dispersion

measurements were done during two different study periods with the initial measurements being done at the tune values of 19.38 and 19.61. These measurements indicated that the dispersion did go down as the tune was increased. In a later study period the data at 19.42 and 19.47 were taken. These results were not consistent with what we had expected or previously observed. This subject will receive additional attention as study time allows.

5.3 Operation of Main Ring at tunes of 19.6

The previous section presents the results of dispersion measurements with both the horizontal and vertical tune around 19.6. Although there is no motivation based on previous simulations why the *dynamic aperture* should be larger with the tunes above the half, we decided to make the measurement anyway.

Tuning was done to obtain the best equilibrium lifetimes in the two regions in the tune plane shown in Figure 20. Again it was observed that operating on the fifth integer resonance lines caused a reduction in dynamic aperture. The equilibrium emittances and lifetimes are shown below.

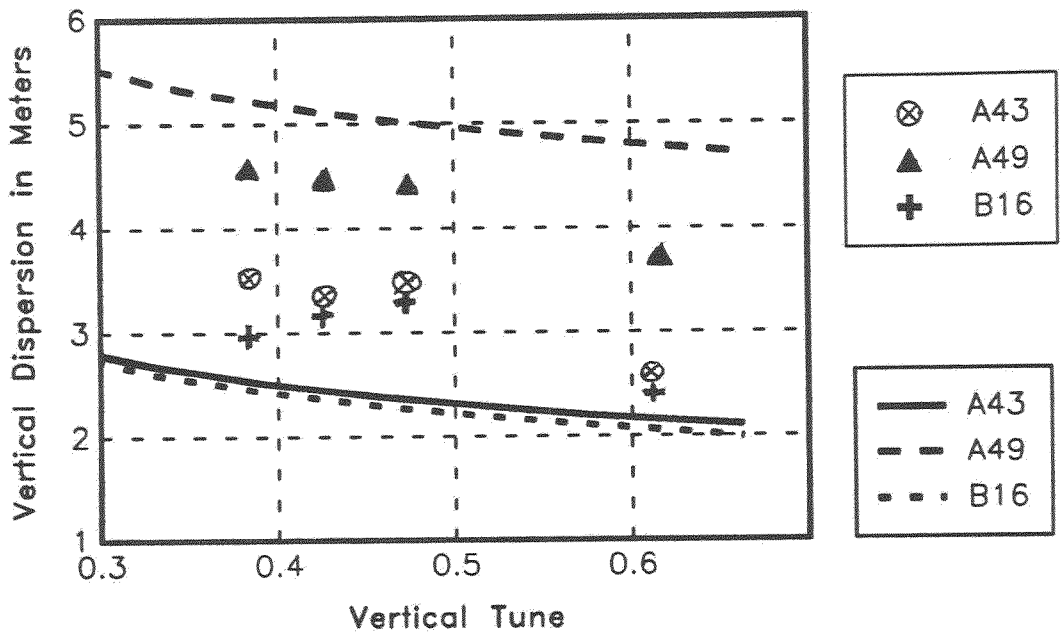

Figure 19: Measured (markers) and Calculated (curves) vertical dispersion at three points in the ring as a function of vertical tune.

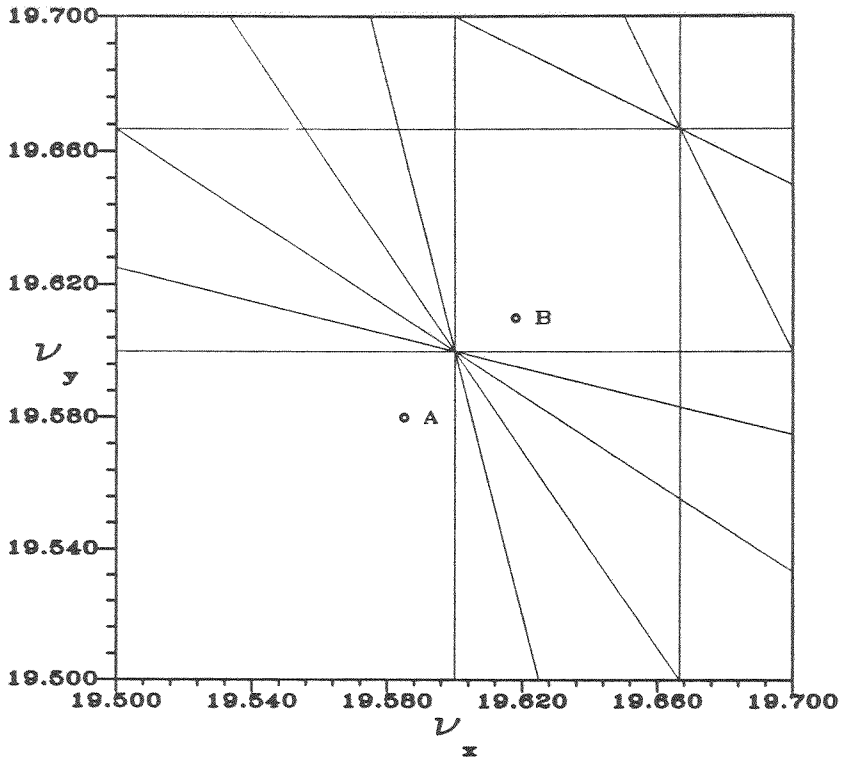

Figure 20: The tune plane above the half integer. The best locations above and below 19.6 are indicated.

Measurement	Lifetime	ϵ_H/π	ϵ_V/π
Point A	46 sec.	10.8 mm-mrad	10.0 mm-mrad
Point B	73 sec.	12.3 mm-mrad	12.8 mm-mrad

6 Operation of Main Ring at 15 GeV/c

Fermilab has made a proposal to replace the Main Ring with a new machine in a separate tunnel. This machine, referred to as the Main Injector, would have approximately half the radius of the Main Ring, and half the number of dipoles. Thus the dipole field would be twice that of the Main Ring. In exploring the issue of dynamic aperture requirements for the Main Injector we attempted some measurements of Main Ring dynamic aperture at 15 GeV/c. This is close to the field that will be required in the Main Injector for injection at 8 GeV. (Note that the injection energy into Main Ring is 8 GeV *kinetic* energy corresponding to a momentum of 8.8889 GeV/c. The 15 GeV/c studies were done at a momentum of 15 GeV/c). Furthermore, magnet measurements have been made on the Main Ring dipoles at the current associated with the 15 GeV/c field. Thus we can eventually compare the measurements with simulations, although this has not yet been done.

Two questions were to be explored; we desired both physical and dynamic aperture

measurements in both transverse planes.

6.1 Physical Aperture Measurements

The physical acceptance is not expected to be a function of energy. However, if the quoted acceptance is normalized to momentum, as it was in Sec 2.1, the actual number will be larger at 15 GeV/c by the ratio of 1.687. The experiment was done using the same techniques used at 8 GeV and again the horizontal aperture was found to be $x_o = 16mm$, consistent with the 8 GeV measurement. In this case the normalized admittance is $41\pi mm - mrad$. Again the vertical admittance could not be measured due to insufficient kicker voltage.

6.2 Dynamic Aperture Measurements

The techniques used in measuring dynamic aperture at 15 GeV/c are similar to those used at 8 GeV. Several problems made the measurement more difficult. As mentioned earlier, it was not possible to turn the rf feedback loops off. As the beam intensity decreased, the loops would encounter a particular intensity that was on the edge of their dynamic range, and they would then influence the beam causing additional beam loss. Secondly, because of the larger dynamic aperture at 15 GeV/c, the natural diffusion due to beam gas scattering was not enough to cause the beam to grow to the dynamic aperture in the available time. Attempts were made to lengthen the cycle, but this proved to be impossible on the time scale of the studies shifts. What did seem to work was an attempt to introduce noise into the Main Ring slow damper system. This is a technique which is often used in the Tevatron but had not previously been used in the Main Ring. The noise did increase the rate of emittance growth, but it also produced accelerated beam loss, particularly when considering the problems with the rf feedback loops. What resulted was a situation in which the emittance was indeed growing, but by the time it approached the dynamic aperture the intensity was often too small to get profile measurements. The numbers presented here are then considered to be lower limits. The table indicates the largest measured beam distributions at 15 GeV/c as well as the largest emittance measurements taken at 8 GeV renormalized to 15 GeV/c.

Measurement	ϵ_H/π	ϵ_V/π
Largest observed emittances at 15 GeV/c	17 mm-mrad	21 mm-mrad
8 GeV dynamic aperture scaled to 15 GeV/c	16.5 mm-mrad	24 mm-mrad

We would expect that the dynamic aperture at 15 GeV/c would be better than what is obtained from scaling, due to the improvement in the magnetic field quality. Thus either the measurements did not allow sufficient time for the equilibrium emittance to develop, or the dynamic aperture is worse than expected.

Table 3: Lifetime in seconds and Dynamic aperture in mm-mrad

Measurement	Lifetime	ϵ_H/π	ϵ_V/π
RF at normal voltage			
$\nu_H = .44, \nu_V = .425$	56	9.8	14.3
$\nu_H = .59, \nu_V = .56$	46	10.8	10.0
$\nu_H = .62, \nu_V = .61$	73	12.3	12.8
15 GeV/c	280	17	21
RF at 20 kv			
$\nu_H = .44, \nu_V = .425$	152	8.2	12.5
$\nu_H = .59, \nu_V = .56$	55	*	*
$\nu_H = .62, \nu_V = .61$	110	*	*

* indicates that data were not taken

7 Concluding Remarks

In this series of experiments considerable progress was made in understanding how to measure the dynamic aperture of Main Ring. The processes of emittance growth were studied and the conclusion was made that the observed growth can be explained by beam-gas scattering. Furthermore the growth rate does not seem to be an operational concern. In order to measure the dynamic aperture one must wait at the injection energy of 8 GeV for about 40 seconds. Then the dynamic aperture is seen to be less than the physical aperture as was expected.

Attempts to pinpoint specific locations in the ring as the cause of the limited dynamic aperture were not successful. It appears that the distributed systematic field errors in the Main Ring dipoles are the reason for the limitation in the dynamic aperture.

These studies also address the question of dynamic aperture at 15 GeV/c. This energy was chosen because the field is similar to the injection field in the proposed Main Injector. We had anticipated a considerable increase in the dynamic aperture over that which was measured at 8 GeV. However, due to the fact that this is an energy at which the Main Ring does not normally sit DC, problems were encountered which make the results questionable. The results were considerably smaller than expected, and it is hoped that further studies after these problems are resolved will yield more consistent results.

Finally, the shorter term behavior (i.e., first 5 seconds) seems to be a consequence of the momentum spread of the beam rather than a limitation due to dynamic aperture. In hopes of improving present operation the question of measuring and reducing dispersion (particularly in the vertical plane) was considered. Plans are being made to implement the tunes of 19.6 in the next fixed target run, and other methods intended to lower the horizontal dispersion are under investigation.

Table 3 summarizes the dynamic aperture measurements.